IEEE Access
Multidisciplinary | Rapid Review | Open Access Journal

Received July 12, 2018, accepted August 18, 2018, date of publication August 23, 2018, date of current version October 8, 2018.

Digital Object Identifier 10.1109/ACCESS.2018.2866875

Research on Inductance Unbalance and Thrust Ripple Suppression of Slot-Less Tubular Permanent Magnet Synchronous Linear Motor

QIANG TAN[1], (Student Member, IEEE), XUZHEN HUANG[2], (Member, IEEE), LIYI LI[1], AND MINGYI WANG[1], (Member, IEEE)

[1]Department of Electrical Engineering, Harbin Institute of Technology, Harbin 150001, China
[2]Department of Electrical Engineering, Nanjing University of Aeronautics and Astronautics, Nanjing 211111, China

Corresponding author: Liyi Li (liliyi.hit@gmail.com)

This work was supported in part by the State Key Program of National Natural Science of China under Grant 51537002, in part by the National Natural Science of China Youth Fund under Grant 51707046, and in part by the State Major Program of National Natural Science of China under Grant 51690182.

ABSTRACT Affected by the end effect, the inductances of the slot-less tubular permanent magnet synchronous linear motor (TPMSLM) are unbalanced. This paper reports the research on the inductance unbalance and the thrust ripple characteristics for the slot-less TPMSLM, and it presents an optimization scheme adopting modular structure with a three-segment primary component. The inductance unbalance characteristic is obtained and quantitatively investigated based on the finite element models. The causes of the self-inductance unbalance and the mutual-inductance are explained, respectively, and the difference between the two unbalances are quantitate investigated. Then, the thrust ripple is specifically analyzed by establishing the voltage and thrust models according to the laws of the inductance unbalance. Thus, the theoretical connection between the inductance unbalance and the thrust ripple has been established. Moreover, the inductance and thrust ripple characteristics of the modular motor are discussed and compared with those of the conventional motor. The prototypes of the conventional motor and the modular motor are developed to verify the findings of the research. At last, corresponding conclusions obtained by the comparison of modular motor with conventional motor are drawn.

INDEX TERMS Inductance, linear motor, permanent magnet, thrust ripple.

NOMENCLATURE

τ	Pole pitch (mm)
τ_s	Virtual slot pitch (mm)
D_e	External diameter of primary component (mm)
D_s	Inner diameter of windings (mm)
D_c	External diameter of secondary component (mm)
D_i	Inner diameter of secondary component (mm)
g	Air-gap length (mm)
b_m	Width of permanent magnet (mm)
h_m	Height of permanent magnet (mm)
h_s	Height of virtual slot (mm)
L_{aa}, L_{bb}, L_{cc}	Three-phase self-inductances (μH)
L''_{cc}	Virtual self-inductance of phase C (μH)
L_0	Average value of self-inductance
L_1	Amplitude of self-inductance
M_{ab}, M_{ac}, M_{bc}	Three-phase mutual-inductances (μH)
M''_{ab}	Virtual mutual-inductance between phase A and B (μH)
M_0	Average value of mutual-inductance
M_1	Amplitude of mutual-inductance
i_a, i_b, i_c	Phase current (A)
I_m	Amplitude of phase current
v	Rated velocity (m/s)

I. INTRODUCTION

Owing to its simple structure, no transverse end effect, and high utilization of the winding, the slot-less tubular permanent magnet linear synchronous motor (TPMSLM) shows a wide application prospect in the linear drive field, especially in the field of precision servo control [1]–[3]. The high

precision application of the slot-less TPMSLM puts forward a very high requirement for the thrust characteristic and mathematical model precision. However, the inductances of the slot-less TPMSLM are unbalanced due to the end effect, and, as a result, the mathematical model becomes more complex and the thrust performance is deteriorated. Hence, to improve the performance and widen the application for the motor, the disadvantage of the inductance unbalance must be overcome.

There exist researches that have focused on the inductance unbalance for motor operation under special conditions [4]–[6]. In [4], a general method based on a permeance network is presented to calculate the unbalanced inductance for the motor under fault conditions. In [5], for the multi-segment permanent magnet synchronous linear motor (PMSLM), the cross-coupling inductance with mover position are examined quantitatively by the acquisition of asymmetrical phase inductances, which are of great significance to establish accurate mathematical model. In [6], based on the unbalanced phenomenon and discipline of mutual inductances, the unbalance mechanism of the asynchronous induction linear motor is analyzed by electromagnetic field theory. These researches have improved inductance model based on different inductance unbalance laws, therefore, the models and conclusions have certain limitations.

For the permanent magnet synchronous linear motor (PMSLM), the influence of the inductance unbalance consists of three aspects. The first is that there is unbalanced current flowing to the inside of the parallel circuit of each phase, and that an extra winding loss is produced [7]. The second is that the mathematical model of the motor becomes more complex and the difficulty of the control algorithms is increased [4], [8], [9]. Due to the inductance unbalance, the d-axis and the q-axis windings cannot be decoupled completely, and the harmonic components in the d-axis and the q-axis self-inductances are increased. The third and most important point is that the drawbacks of the inductance unbalance can cause additional thrust fluctuation, impeding a further improvement in positioning accuracy [8], [10].

Thrust characteristic is the most important characteristic of linear motor, so the influence of inductance unbalance cannot be ignored. For the flat plate type PMSLM, a method of setting auxiliary teeth is proposed to reduce the three-phase inductance unbalance [7]. However, this method requires an optimum design of the dimensions, which is blind to carry out, and the mutual-inductance unbalance cannot be suppressed effectively. Except for that, in [11], the inductance unbalance is suppressed by adopting a modular primary iron-core structure, in which each slot of the PMSLM is separated. However, this structure has resulted in a certain volume waste and increased the difficulty of the processing. Moreover, it is regrettable that no theoretical connection between the inductance unbalance and the thrust ripple has been established in these two papers.

The above two optimization methods can provide references, but they cannot be applied to the design of the slot-less TPMSLM directly. The reason is that there is a distinct difference between the slot-less TPMSLM and the flat PMSLM. For the slot-less TPMSLM, the circular coil in a single slot (or virtual slot for the slot-less motor) can form an effective conductor [12], [13]. This specific characteristic causes the winding and core structures of the motor to be more diverse. In addition to that, the unbalance of the mutual-inductance is more prominent than that of the self-inductance, due to its special sole-less structure. Considering these specific characteristics, the inductance unbalance and the thrust ripple characteristics of the slot-less TPMLSM are investigated in this paper.

In Section II, the inductance unbalance of the motor is analyzed in detail, and its law is analyzed by finite element (FEM) simulation. In Section III, the thrust ripple of the TPMSLM is analyzed. The influence of the inductance unbalance on the thrust ripple is studied quantitatively by developing the voltage and thrust models. To suppress the inductance unbalance and the thrust ripple, a type of modular structure with a three-segment primary component is proposed in Section IV. The prototype of the conventional motor and the modular motor are developed to experimentally verify the findings of this paper in Section V. Finally, corresponding conclusions are drawn in Section VI.

II. ANALYSIS OF THE INDUCTANCE UNBALANCE

A. STRUCTURE AND PARAMETERS OF THE SLOT-LESS TPMSLM

Fig. 1 shows the structure diagram of a 24-slot-8-pole slot-less TPMSLM. The motor contains one primary and one secondary components. In the primary component, the annular windings are arranged according to the phase sequence, and they are set in the inner of the tubular primary iron. The permanent magnets (PMs) and the secondary irons are sleeve-jointed in sequence on the non-magnetic axis in the secondary component. The motor has no teeth, forming a large equivalent air gap, thus the armature reaction is very slight [14]. The structural parameters of the motor are listed in Table 1.

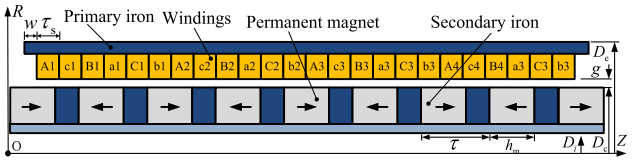

FIGURE 1. Conventional slot-less TPMSLM.

B. OTHER RECOMMENDATIONS

For the slot-less TPMSLM, the longitudinal end effect has different influences on the self-inductance and the mutual-inductance unbalances. Hence, the self-inductance and the mutual-inductance unbalances are analyzed respectively from two aspects: magnetic circuit reluctance and coils space distribution.

TABLE 1. Structure parameters.

Symbol	Items	Parameters
D_e	External diameter of primary iron	85 mm
D_s	Inner diameter of windings	60 mm
D_c	External diameter of secondary component	58.4 mm
D_i	Inner diameter of secondary component	16.4 mm
τ	Pole pitch	25.5 mm
τ_s	Virtual slot pitch	8.5 mm
g	Length of air-gap	0.8 mm
b_m	Weight of permanent magnet	16 mm
h_m	Height of permanent magnet	15.5 mm
N	Number of turns per coil	15 mm

The self-inductance is inversely proportional to the reluctance of the magnetic circuit [15]. The magnetic saturation degree of the end-iron is different from that of the non-end-iron, and so the magnetic reluctance of the three-phase magnetic circuits is unbalanced, which eventually leads to the self-inductance unbalance [10]. As shown in Fig. 1, coil A1 at the left end belongs to phase A, whereas coil b3 at the right end belongs to phase B, therefore, the self-inductances of phases A and B are different from those of phase C.

Different from the self-inductance, the unbalance of the mutual-inductance is mainly affected by the space distribution of the winding coils. The coupling between the end coil and the other coils is different from that between the non-end coil and the other coils. Therefore the mutual-inductance becomes unbalanced. It can be seen from Fig. 1 that the coupling degree between phases A and B is weaker than both that of phases A and C, and that of phases B and C. Therefore, the mutual-inductance between phases A and B is smaller than that between phases A and C, as well as that between phases B and C.

The inductance characteristic of the motor is obtained by FEM simulation. Both the no-load and load models are established and analyzed. In the no-load model, the windings are open without current, whereas, in the rated load model, the sinusoidal currents are electrified. Since the armature reaction is very slight, the inductance characteristic when the motor is no-load is almost the same as that when the motor is loaded. The inductance waveforms of the motor under no-load condition are shown in Fig. 2. What needs to be specified is that in order to highlight the law of the inductance unbalance, two hypothesized parameters (L''_{cc} and M''_{ab}) are assumed in this section: L_{cc} is the virtual self-inductance of phase C, which is balanced with L_{aa} and L_{bb}, whereas M''_{ab} is the virtual mutual-inductance between phases A and B, which is balanced with M_{ac} and M_{bc}.

As shown in Fig.2 (a), the balanced three-phase inductances composed of L_{aa}, L_{bb} and L''_{cc} fluctuate from 220.8 μH to 232.6 μH, whereas the actual L_{cc} fluctuates from 221.8 μH to 233.8 μH. As shown in Fig.2 (b), the balanced three-phase mutual-inductances composed of M''_{ab}, M_{ac} and M_{bc}

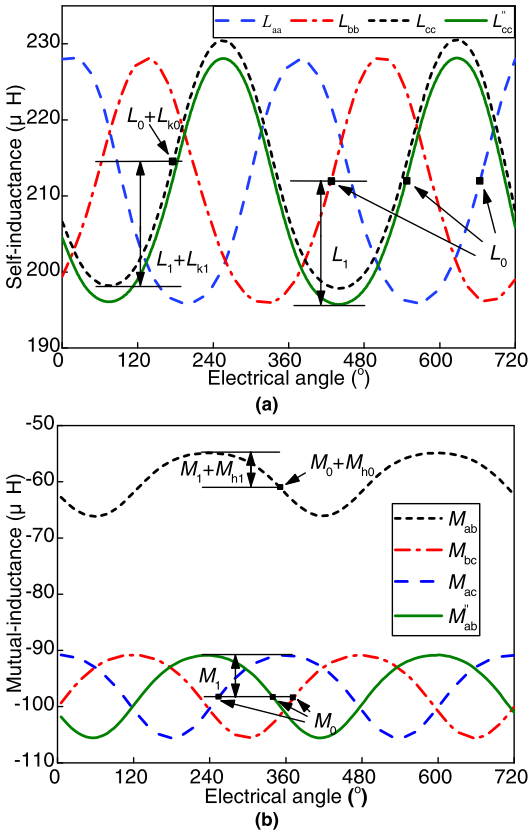

FIGURE 2. Inductance waveforms of the conventional slot-less TPMSLM. (a) Self-inductance; (b) Mutual-inductance.

fluctuate from -89.4 μH to -103.8 μH, whereas the actual M_{ab} fluctuates from -56.7μH to -67.9 μH. The above results show that the average value and amplitude of L_{cc} are different from those of L_{aa} and L_{bb}, and that the average value and amplitude of M_{ab} are different from those of M_{ac} and M_{bc}. Additionally, we can observe from Fig. 2 that the phase differences between any two-phase inductances are the same.

The differences among the average values and the amplitudes of the three-phase inductances indicate the extent of the inductance unbalance. For convenience analysis, the parameters are specified as follows: L_{k0} is the difference among the average values of L_{aa}, L_{bb} and L_{cc}; L_{k1} is the difference among the amplitudes of L_{aa}, L_{bb} and L_{cc}; M_{h0} is the difference among the average values of M_{ab}, M_{ac} and M_{bc}; M_{h1} is the difference among the amplitudes of M_{ab}, M_{ac} and M_{bc}.

When the motor is loaded, the values of L_{k0}, L_{k1}, M_{h0}, and M_{h1} are 1.1 μH, 0.1 μH, 34.3 μH, and 1.6 μH, respectively, as shown in Fig. 2. In order to analyze the influence of the armature reaction on the inductance unbalance, the curve of the inductance differences varying with the armature current is obtained by FEM simulation, as shown in Fig. 3. From the simulation results we can observe that L_{k0}, L_{k1}, M_{h0} and M_{h1} are all independent from the armature current and remain constant as the armature current increases. Also, M_{h0} is much larger than L_{k0}, L_{k1} and M_{h1}. This indicates that the degree of

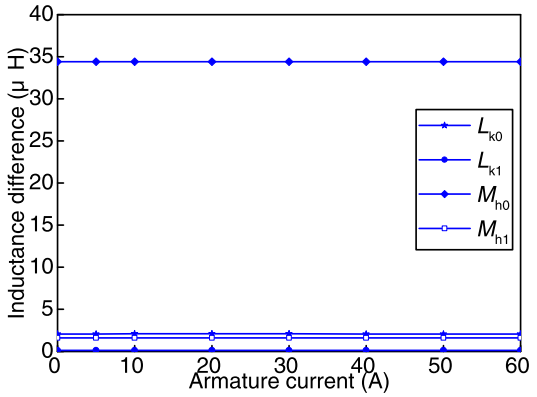

FIGURE 3. Variation of the inductance differences with the armature current.

the mutual-inductance unbalance is much larger than that of the self-inductance unbalance.

III. ANALYSIS OF THE THRUST RIPPLE

Without considering external disturbance, the thrust ripple of the PMSLM can be divided into two parts: detent force and thrust fluctuation [16]. The detent force composed of the cogging force and the end force is independent of the armature current [17], [18]. The thrust fluctuation, which is caused by armature current unbalance, armature current harmonic, armature voltage unbalance and armature voltage harmonic, is related to the armature current [19], [20]. Not affected by the cogging effect, the back electromotive force (EMF) waveform is sinusoidal and the harmonic contents of armature voltage can be ignored for the slot-less TPMSLM. To simplify the analysis model of the thrust fluctuation, the motor is supplied by the ideal three-phase sinusoidal alternating currents. In this case, the mainly cause of the thrust fluctuation for the motor is the armature voltage unbalance.

A. SUPPRESSION OF THE NO-LOAD BACK EMF UNBALANCE

The armature voltage of the motor consists of three parts: the resistive voltage drop, the inductive voltage drop, and the no-load back EMF [21]. To study the influence of the inductance unbalance on the thrust fluctuation, the unbalance of the three-phase no-load back EMF should be suppressed first. In [22], optimizing the length of the primary end-iron is done to suppress the no-load back EMF unbalance. This method is used for the slot-less TPMSLM in this paper, as shown in Fig. 4.

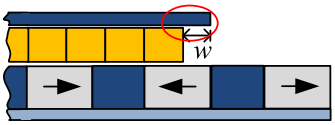

FIGURE 4. Optimization of the end-iron length in the primary component.

Fig. 5 shows the amplitudes of the three-phase no-load back EMFs varying with the length of the primary end-iron, which is designed to be 9 mm after optimization. As a result, the three-phase no-load back EMF waveforms almost achieve balance, in which the differences among three-phase amplitudes are less than 0.03V, as shown in Fig.6.

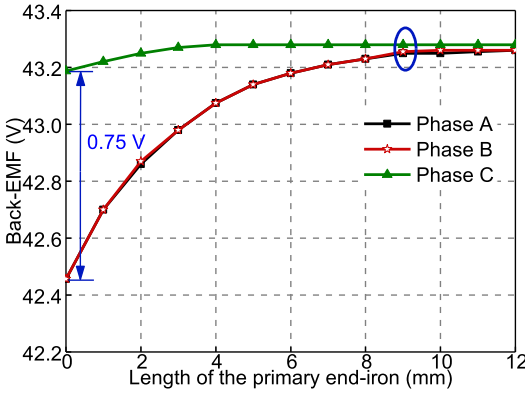

FIGURE 5. Back EMFs varying with the length of primary end-iron.

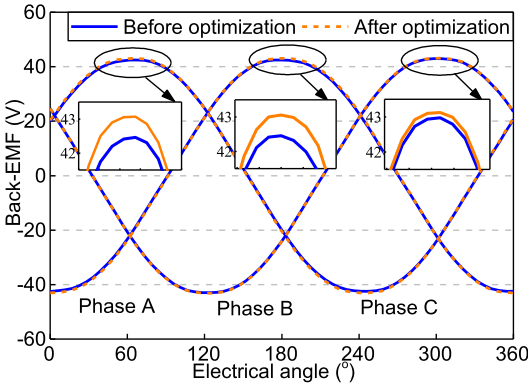

FIGURE 6. Three-phase back EMF waveforms before and after optimization.

B. THRUST FLUCTUATION CAUSED BY THE INDUCTANCE UNBALANCE

After the optimization as shown in Fig. 4, the main cause of the armature voltage unbalance for the slot-less TPMSLM is the inductance unbalance. Thus the thrust fluctuation can be calculated directly by the unbalanced inductances.

The actual three-phase inductances can be divided into two parts: one is the balanced three-phase inductances, composed of L_{aa}, L_{bb}, L''_{cc}, M''_{ab}, M_{ac}, and M_{bc}; the other is the additional inductances, composed of L_{scc} and M_{sab}. The balanced three-phase inductances will not cause the thrust fluctuation, so only the additional inductances need to be considered when calculating the thrust fluctuation. The additional inductances can be expressed by:

$$L_{scc} = L_{cc} - L''_{cc} = L_{k0} + L_{k1}\cos(2\omega t - 2\pi/3) \quad (1)$$

$$M_{sab} = M_{ab} - M''_{ab} = -M_{h0} - M_{h1}\cos(2\omega t - 2\pi/3) \quad (2)$$

where ω is the angular velocity ($\omega = \pi v/\tau$). The initial position angle is defined as 0° when the winding axis of phase A is aligned in the secondary flux axis.

The three-phase armature voltage influenced by the additional inductances can be calculated by:

$$\begin{cases} e_{sa} = \dfrac{d\psi_{sa}}{dt} = \dfrac{d(0\cdot i_a + M_{sab} i_b + 0\cdot i_c)}{dt} = \dfrac{d(M_{sab} i_b)}{dt} \\ e_{sb} = \dfrac{d\psi_{sb}}{dt} = \dfrac{d(M_{sab} i_a + 0\cdot i_b + 0\cdot i_c)}{dt} = \dfrac{d(M_{sab} i_a)}{dt} \\ e_{sc} = \dfrac{d\psi_{sc}}{dt} = \dfrac{d(0\cdot i_a + 0\cdot i_b + L_{scc} i_c)}{dt} = \dfrac{d(L_{scc} i_c)}{dt} \end{cases} \quad (3)$$

The thrust fluctuation caused by the additional inductances can by represented as:

$$\begin{aligned} f_s &= \frac{(e_{sa} i_a + e_{sb} i_b + e_{sc} i_c)}{v} \\ &= \frac{\pi I_m^2}{2\tau}(L_{k0} - 2L_{k1} - 2M_{h0} - 2M_{h1})\sin\left(2\omega t - \frac{2\pi}{3}\right) \\ &\quad + \frac{3\pi I_m^2}{4\tau}(L_{k1} - 2M_{h1})\sin\left(4\omega t + \frac{2\pi}{3}\right) \end{aligned} \quad (4)$$

The thrust fluctuation caused by the inductance unbalance can be divided into two parts as follows: one is the 2nd harmonic component, caused by L_{k0}, L_{k1}, M_{h0}, and M_{h1}; the other is the 4th harmonic component, caused by the L_{k1} and M_{h1}. When the armature current is small, the thrust fluctuation can be ignored. However, when the motor is loaded, the average thrust is proportional to the armature current, whereas the thrust fluctuation is proportional to the square of the armature current. As a result, the ratio of the thrust ripple to the average thrust increases as the armature current increases.

IV. MODULAR STRUCTURE WITH THE THREE-SEGMENT PRIMARY COMPONENT

A. MODULAR STRUCTURE WITH THREE-SEGMENT PRIMARY COMPONENT

The modular structure with a three-segment primary component is proposed in this section to reduce the inductance unbalance and the thrust fluctuation, as shown in Fig. 7. The primary of the motor is initially divided into three independent segments (I, II and III), which are separated by air or connected by a non-magnetic flux barrier. The total width of the flux barrier and the two end teeth is one pole pitch τ. Compared with the conventional motor, segment II is shifted by one pole pitch along the axial direction, so the electrical angle increases 180° and the connection direction of the windings in segment II needs to be reversed. Segment III is shifted by two time pole pitches, so the electrical angle increases 360°, and the connection direction of the windings in segment III remains unchanged.

Considering that the flux barriers occupy some space, the thrust density (the ratio of the average thrust to the volume) therefore decreases, and the modular structure can be improved further by setting the auxiliary end teeth [16]. As shown in Fig. 7, the teeth are set at both ends of each segmental primary iron. In order to achieve the low detent force, the number of the virtual slots in the primary component is optimally designed as 21. Despite this, these parameters differences between the conventional motor and the modular motor will not affect the suppression effect of the inductance unbalance.

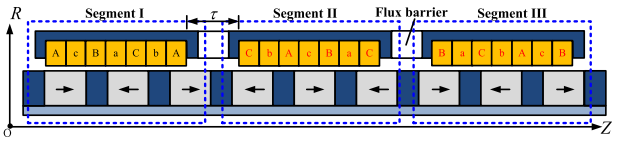

FIGURE 7. Modular structure with three-segment primary component.

B. ANALUSIS OF THE INDUCTANCE CHARACTERISTIC

The FEM simulation models of the three segmental motors and the whole motor are established. The inductances of the segmental motors are listed in Table 2.

TABLE 2. Inductance of the three segmental motors.

Parameter	Segment I	Segment II	Segment III
L_{aa} (μH)	83.5~95.2	59.6~66.7	59.6~66.7
L_{bb} (μH)	59.6~66.7	59.6~66.7	83.5~95.2
L_{cc} (μH)	59.6~66.7	83.5~95.2	59.6~66.7
M_{ab} (μH)	-21.1~-22.6	-34.5~-36.3	-21.1~-22.6
M_{ac} (μH)	-21.1~-22.6	-21.1~-22.6	-34.5~-36.3
M_{bc} (μH)	-34.5~-36.3	-21.1~-22.6	-21.1~-22.6

For segment I, L_{aa} is larger than L_{bb} and L_{cc}, whereas M_{bc} is larger than M_{ab} and M_{ac}; for segment II, L_{cc} is larger than L_{aa} and L_{bb}, whereas M_{ab} is larger than M_{bc} and M_{ac}; and for segment III, L_{bb} is larger than L_{aa} and L_{cc}, whereas M_{ac} is larger than M_{ab} and M_{bc}. For all that, the more important rule is that the values of the larger phase inductances in the three segmental motors are the same, and the values of the smaller phase inductances in the three segmental motors are also the same. The three-phase inductances of the whole motor are the sum of those for the three segmental motors. Therefore, the three-phase inductances of the whole motor achieve balance: the three-phase self-inductances all fluctuate from 202.7 μH to 228.6μH, whereas the three-phase mutual-inductances all fluctuate from −76.7 μH to −81.5 μH.

When the motor is with rated load, the three-phase armature voltages become balanced after the suppression of the inductance unbalance. Fig 8 shows the waveforms of the three-phase armature voltages for the two motors. For the modular motor, the three-phase armature voltages achieve balance, in which the amplitudes are all 45.72 V and the phase differences are all 120°. On the other hand, the armature voltages of the conventional motor are obvious unbalanced due

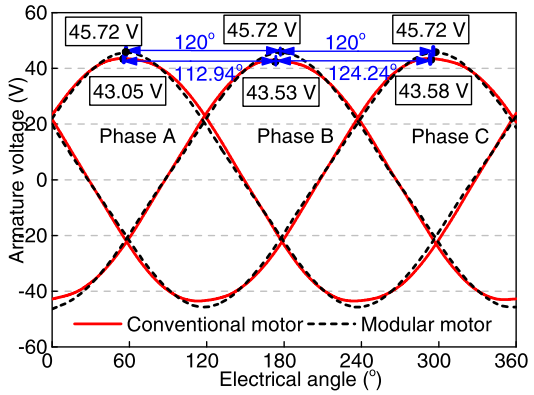

FIGURE 8. Three-phase armature voltages of the two motors.

to the inductance unbalance: the amplitudes of three-phase armature voltage are 43.05 V, 43.53 V, and 43.58 V, respectively; the phase differences between any two of them are 112.94°, 124.24°, and 112.82°, respectively.

For the modular structure, the primary component is divided into three segments, so the number of the primary ends increases from two to six. The coils in the six ends belong to the three-phase windings. The magnetic resistances of the three phases are the same, thus, the self-inductances of the three phases are balanced. When it comes to the coil distribution, the coupling coefficients among the three-phase coils are the same, therefore, the mutual-inductances of the three phases can also be balanced. The modular structure with a three-segment primary component realizes balance in magnetic resistance and winding distribution, thereby solving the problem of the inductance unbalance.

C. COMPARATIVE ANALYSIS OF THE THRUST CHARACTERISTIC

On the premise of the same secondary length, the parameters of the conventional motor and the modular motor are compared, including weight, volume, thrust, acceleration and so on. The specific parameters are listed in Table 3.

TABLE 3. Parameters of the two motors.

Parameter	Conventional	Modular
Weight of the primary component (kg)	5.78	5.37
Weight of the winding (kg)	3.32	2.91
Length of the primary component (mm)	222	236
Acceleration (m/s^2)	59.5	66.5
Rated current (A)	30	30
Rated thrust (N)	344	357

Three conclusions can be drawn: not considering the weight of the flux barrier, the weight of the modular motor is 7% lighter than that of the conventional motor; the primary component length of the modular motor is 6.3% longer than that of the conventional motor due to the existence of the flux barrier; and the average thrust of the modular motor is 3.8% larger than that of the conventional motor owing to the auxiliary end teeth.

Moreover, the thrust ripple characteristics of the two motors have a clear distinction. Fig. 9 shows the detent force waveforms. We can observe that the modular motor's detent force is just 7.2 N, 83.18% lower than that of the conventional motor, which is due to the suppression effect of the modular structure. Also, the cycles of the detent force for the conventional motor and the modular motor are one pole pitch and one-third pole pitch respectively, which is consistent with the research results in [23].

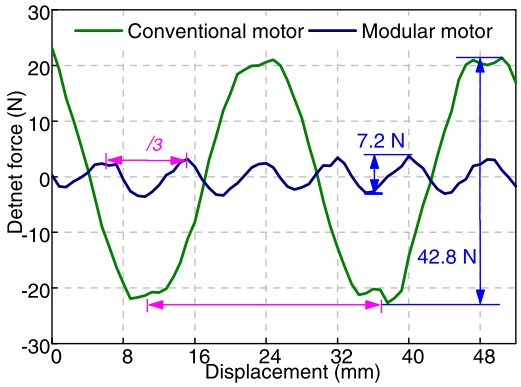

FIGURE 9. Detent forces of the two motors.

The load thrust curves for these two motors are shown in Fig.10. When the armature current increases from 5A to 15 A, the thrust curve variations of the two motors are different: the peak-to-peak value of the thrust ripple for the conventional motor increases from 43.2 N to 51.4 N, and the curve of the thrust ripple has also changed obviously due to the additional thrust fluctuation; the thrust ripple curve of the modular motor is almost invariable, representing only a small increase in the amplitude. This indicates that the influence of the additional thrust fluctuation is very slight through the modular design.

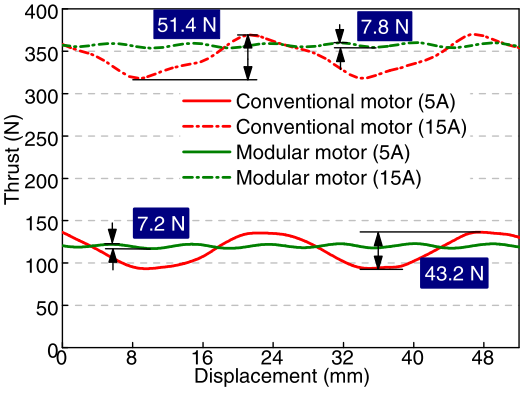

FIGURE 10. Thrust curves of the two motors.

Moreover, the curves of the thrust ripple peak values' variation with the armature current are shown in Fig. 11. As the armature current increases, the thrust ripple of the conventional motor increases whereas that of the modular motor remains constant. When the current is at rated value, about 15A, the thrust ripple peak values of the conventional motor

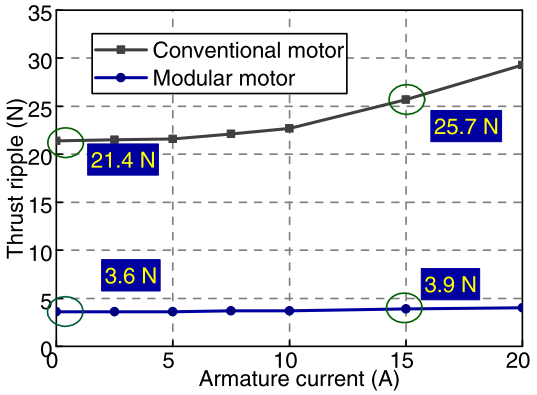

FIGURE 11. Thrust ripples of the two motors variation with armature current.

and the modular motor are 25.7 N and 3.9 N respectively, in which the latter is 84.8% less than the former. It is the case that not only the detent force of the modular motor is very small, but also the additional thrust fluctuation is almost absent.

The inductance characteristics shown in Table 2 and the thrust ripple characteristics shown in Figs. 10 and 11 indicate that the modular structure with the three-segment primary component can suppress the inductance unbalance effectively, and thus suppress the thrust fluctuation caused by the inductance unbalance effectively.

V. EXPERIMENTAL VERIFICATION

The prototypes of the conventional and the modular motors are developed to experimentally verify the research findings presented in this paper, as shown in Fig. 12. The flux barrier in the modular motor is constructed of aluminum parts. The experiments include inductance and thrust tests.

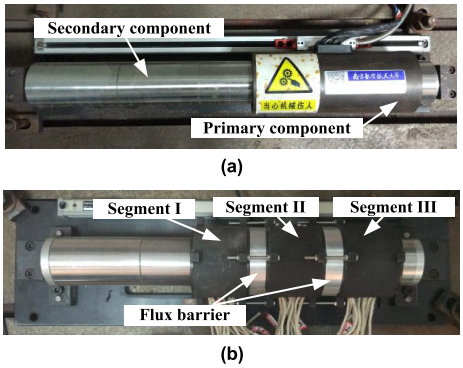

FIGURE 12. Prototypes. (a) Conventional motor; (b) Modular motor.

A. INDUCTANCE TEST

For the slot-less TPMSLM, self-inductance can be tested directly by an LCR test instrument whereas the mutual-inductance needs to be tested indirectly [24]. Any two-phase windings among the three-phase windings are selected, and then these two-phase windings should be connected in series and in reverse, respectively, as shown

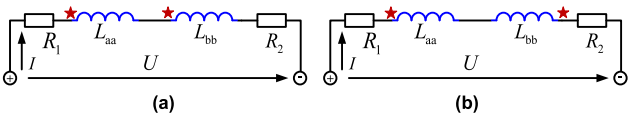

FIGURE 13. Connection diagram. (a) Forward series; (b) Reverse series.

in Fig. 13. The loop inductance in the forward series can be represented as:

$$L_f = L_{aa} + L_{bb} + 2M_{ab} \tag{5}$$

The loop inductance in reverse series can be represented as:

$$L_r = L_{aa} + L_{bb} - 2M_{ab} \tag{6}$$

Therefore, the mutual-inductance between these two-phase windings can be calculated by:

$$M_{ab} = \frac{L_f - L_r}{4} \tag{7}$$

The test process is as follows: the prototype is dragged by the servo electric cylinder in the experiment progress; in the range of two time pole pitches, 25 positions are sampled; in each position, the self-inductance is tested first by using the LCR test instrument; then the two phase-windings are connected in series and in reverse series respectively; the loop inductances are tested by the LCR test instrument and the mutual-inductance is calculated by (7).

Fig.14 shows the inductance waveforms of the prototypes. We can observe that the test inductances are slightly smaller than the simulation values, with maximum deviations of 3.7%, which could well be due to an air gap machining error. More importantly, the laws of the inductance unbalance or balance tested are in agreement with the simulation results. For the conventional motor, the average value of L_{cc} is larger than that of L_{aa} and L_{bb}; the average value of M_{ab} is smaller than those of M_{ac} and M_{bc}; and M_{h0} is much larger than L_{k0}, L_{k1} and M_{h1}. For the modular motor, L_{aa}, L_{bb} and L_{cc} are almost balanced, and the differences among M_{ab}, M_{ac}, and M_{bc} are smaller than 2μH. What needs to be emphasized is that the tested and simulated three-phase mutual-inductances of the modular motor are not all strictly balanced. This is mainly due to the coupling effect between the adjacent segmental motors, which means that the three-phase inductances of the entire motor have a slight difference from the sum calculated for the three segmental motors.

B. THRUST TEST

The detent force characteristics of the two prototypes are obtained, as shown in Fig. 15. As the mover travels two times pole pitches, the detent force of the conventional motor fluctuates with two cycles whereas that of the modular motor fluctuates with six cycles. So the cycles of the detent force for the conventional motor and the modular motor are one pole pitch and one-third pole pitch respectively, which is consistent with the analysis presented in Section IV. Moreover, the tested detent force matches closely to the FEM figure,

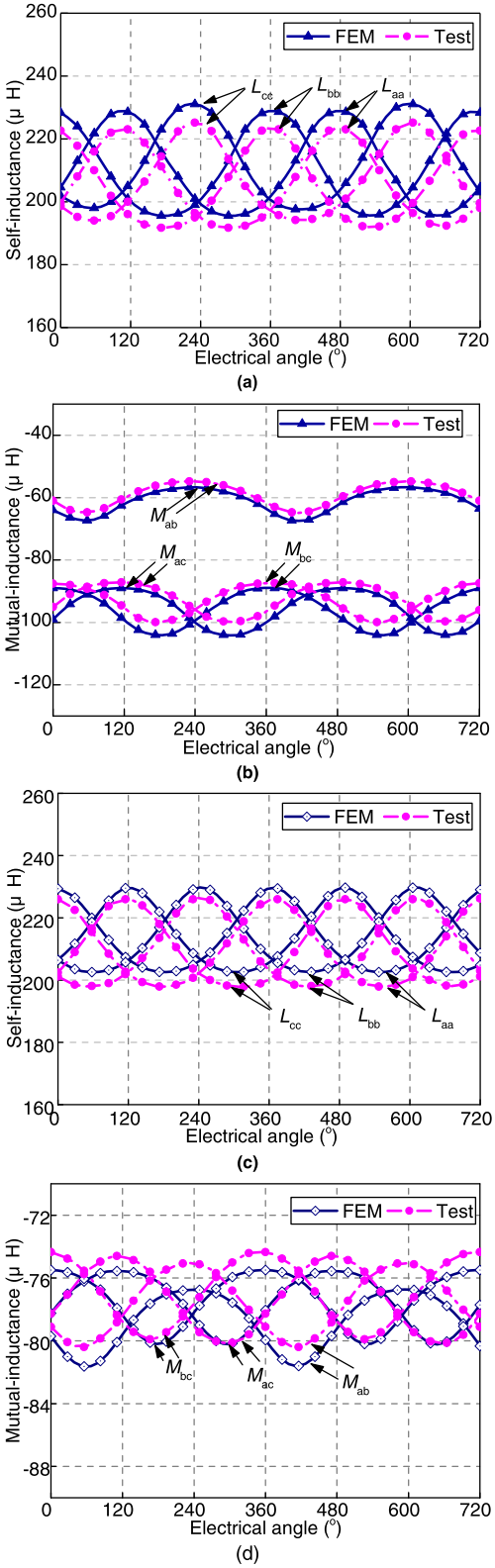

FIGURE 14. Inductance waveforms. (a) Self-inductance of conventional motor; (b) Mutual-inductance of conventional motor; (c) Self-inductance of modular motor; (d) Mutual-inductance of modular motor.

with maximum deviations of 10% and 22% for the conventional motor and the modular motor respectively. There are many reasons for this result, including machining errors,

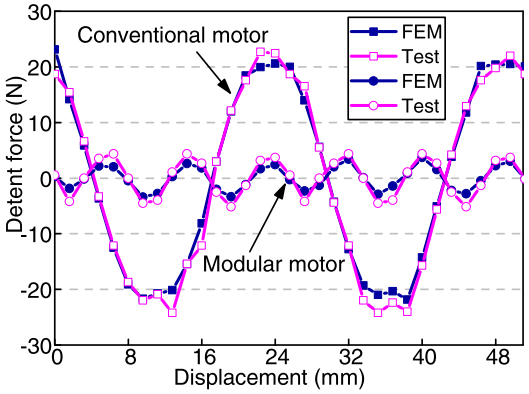

FIGURE 15. Detent force-displacement curves.

impact of friction, inconsistency of the material performance, or precision of the sensor. In conclusion, the experimental results show two points: the detent force of the modular motor is much lower than that of the conventional motor; taking one pole pitch as the cycle, the main content of the detent force for the modular motor is the three harmonic components, whereas that for the conventional motor is the fundamental component.

When the windings are powered with a DC current, the mover can output static thrust, which varies with the mover position as it is dragged. When the thrust is highest, the current is close to the q-axis current, whereas the point of the lowest thrust corresponds to the d-axis position. Fig. 16 shows the variation of the static thrust with the armature current. The test results broadly correspond with the FEM results, with maximum deviations of 4.2%. Additionally, the average thrust of the modular motor is about 3.4% higher than that of the conventional motor, which is consistent with the comparative results in Section IV.

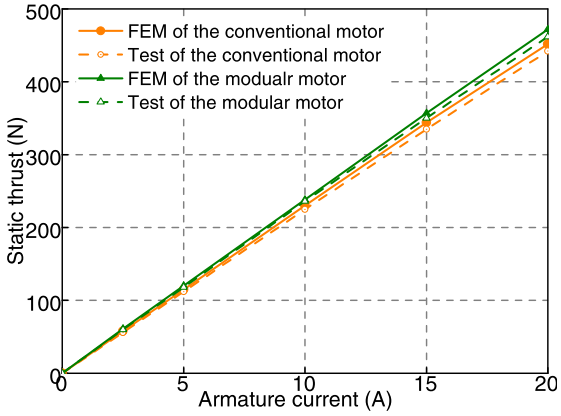

FIGURE 16. Static thrust variation with armature current.

VI. CONCLUSION

The inductance unbalance characteristic of the slot-less TPMSLM is investigated, and a kind of modular structures with three-segment primary components is proposed to suppress the inductance unbalance in this paper. Affected by the longitudinal end effect, the three-phase inductances of the slot-less TPMSLM are asymmetrical, what is special is that the degree of the mutual-inductance unbalance is much

greater than that of the self-inductance unbalance. According to the thrust model established to consider the inductance unbalance, there will be an additional thrust fluctuation component proportional to the square of the armature current, so the thrust performance of the motor is deteriorated.

For the modular structure of the three-segment primary component, the number of the primary component ends increases from two to six. As a result, the magnetic resistance and the coils distribution for the three-phase windings achieve the balance, thus, the three-phase inductance unbalance is effectively suppressed. Naturally, the additional thrust fluctuation caused by the inductance unbalance is also suppressed. Furthermore, the motor with the three-segment primary component can achieve a small detent force owing to the mutual cancellation of the unit detent forces. Through adopting a modular structure and setting auxiliary end teeth, the average thrust of the slot-less TPMLSM is increased by 3.4%, and the thrust ripple is reduced by 84.8%.

The research presented in this paper is experimentally verified by developing the prototypes of the conventional motor and the modular motor. The modular structure proposed in this paper can also be applied to various kinds of slot or slot-less PMLSMs.

REFERENCES

[1] J. Wang and D. Howe, "Tubular modular permanent-magnet machines equipped with quasi-Halbach magnetized magnets—Part I: Magnetic field distribution, EMF, and thrust force," *IEEE Trans. Magn.*, vol. 41, no. 9, pp. 2470–2478, Sep. 2005.

[2] I. I. Abdalla, T. Ibrahim, and N. M. Nor, "Analysis of tubular linear motors for different shapes of magnets," *IEEE Access*, vol. 6, pp. 10297–10310, 2018.

[3] T. Xia, H. Yu, Z. Chen, L. Huang, X. Liu, and M. Hu, "Design and analysis of a field-modulated tubular linear permanent magnet generator for direct-drive wave energy conversion," *IEEE Trans. Magn.*, vol. 53, no. 6, Jun. 2017, Art. no. 8103904.

[4] Z. Bo, Z. Jimin, H. Guiqing, Z. Jibin, and X. Yongxiang, "Asymmetry of inductance and torque ripple of multi-unit permanent magnet synchronous motor," in *Proc. Int. Conf. Elect. Mach. Syst. (ICEMS)*, Hangzhou, China, Aug. 2014, pp. 1–5.

[5] M. Ma, "Investigation of cross-coupling inductances for long-stator PM linear motor arranged in multiple segments," in *Proc. Int. Magn. Conf. (INTERMAG)*, Beijing, China, May 2015, pp. 1–4.

[6] J. Lu and W. Ma, "Investigation of phase unbalance characteristics in the linear induction coil launcher," *IEEE Trans. Plasma Sci.*, vol. 39, no. 1, pp. 110–115, Jan. 2011.

[7] K.-B. Jang, J.-H. Kim, H.-J. An, and G.-T. Kim, "Optimal design of auxiliary teeth to minimize unbalanced phase due to end effect of PMLSM," *IEEE Trans. Magn.*, vol. 47, no. 5, pp. 1010–1013, Oct. 2011.

[8] S. Yamamoto, T. Kano, T. Yamaguchi, H. Hirahara, and T. Ara, "Asymmetric circuit models and parameter measurement for permanent magnet linear synchronous motor considering inductance harmonics," in *Proc. Int. Power Electron. Conf. (ECCE ASIA)*, Sapporo, Japan, Jun. 2010, pp. 1752–1759.

[9] R. G. Rhudy, H. D. Snively, and J. C. White, "Performance of synchronous machines operating with unbalanced armature windings," *IEEE Trans. Energy Convers.*, vol. EC-3, no. 2, pp. 391–397, Jun. 1988.

[10] C. Liu, H. Wang, Z. Zhang, and X. Shen, "Research on thrust characteristics in permanent magnet linear synchronous motor based on analysis of nonlinear inductance," *Chin. Soc. Elect. Eng.*, vol. 31, no. 30, pp. 69–77 Oct. 2011.

[11] Y. Bai, T. Yang, and B. Kou, "Reducing detent force and three-phase magnetic paths unbalance of PM linear synchronous motor using modular primary iron-core structure," in *Proc. Int. Conf. Elect. Mach. Syst. (ICEMS)*, Hangzhou, China, Oct. 2014, pp. 1–4.

[12] N. Bianchi, S. Bolognani, and F. Tonel, "Design criteria of a tubular linear IPM motor," in *Proc. IEEE Int. Electr. Mach. Drives Conf. (IEMDC)*, Cambridge, MA, USA, Jun. 2001, pp. 1–4.

[13] J. Wang, Z. Lin, and D. Howe, "Analysis of a short-stroke, single-phase, quasi-Halbach magnetised tubular permanent magnet motor for linear compressor applications," *IET Electr. Power Appl.*, vol. 2, no. 3, pp. 193–200, May 2008.

[14] X. Huang, Q. Tan, Q. Wang, and J. Li, "Optimization for the pole structure of slot-less tubular permanent magnet synchronous linear motor and segmented detent force compensation," *IEEE Trans. Appl. Supercond.*, vol. 26, no. 7, Oct. 2016, Art. no. 0611405.

[15] Y. Luo and B. Chen, "Improvement of self-Inductance calculations for circular coils of rectangular cross section," *IEEE Trans. Magn.*, vol. 49, no. 3, pp. 1249–1255, Mar. 2013.

[16] X. Z. Huang, J. Li, Q. Tan, Z. Y. Qian, C. Zhang, and L. Li, "Sectional combinations of the modular tubular permanent magnet linear motor and the optimization design," *IEEE Trans. Ind. Electron.*, vol. 65, no. 12, pp. 9658–9667, Dec. 2018.

[17] M. Ma, L. Li, J. Zhang, J. Yu, H. Zhang, and Y. Jin, "Analytical methods for minimizing detent force in long-stator PM linear motor including longitudinal end effects," *IEEE Trans. Magn.*, vol. 51, no. 11, Nov. 2015, Art. no. 8204104.

[18] H. Hu, X. Liu, J. Zhao, and Y. Guo, "Analysis and minimization of detent end force in linear permanent magnet synchronous machines," *IEEE Trans. Ind. Electron.*, vol. 65, no. 3, pp. 2475–2486, Mar. 2018.

[19] S.-L. Chen, K. K. Tan, S. Huang, and C. S. Teo, "Modeling and compensation of ripples and friction in permanent-magnet linear motor using a hysteretic relay," *IEEE/ASME Trans. Mechatronics*, vol. 15, no. 4, pp. 586–594, Aug. 2010.

[20] P. Ponomarev, I. Petrov, and J. Pyrhönen, "Influence of travelling current linkage harmonics on inductance variation, torque ripple and sensorless capability of tooth-coil permanent-magnet synchronous machines," *IEEE Trans. Magn.*, vol. 50, no. 1, Jan. 2014, Art. no. 8200108.

[21] M. Merdzan, S. Jumayev, A. Borisavljevic, K. O. Boynov, J. J. H. Paulides, and E. A. Lomonova, "Electrical and magnetic model coupling of permanent magnet machines based on the harmonic analysis," *IEEE Trans. Magn.*, vol. 51, no. 11, Nov. 2015, Art. no. 8108904.

[22] Q. Wang, B. Zhou, X. Huang, and Q. Tan, "Suppression of leakage flux and thrust ripple for slot-less tubular permanent magnet linear synchronous motor," in *Proc. IEEE Conf. Expo Transp. Electrific. Asia–Pacific (ITEC Asia–Pacific)*, Beijing, China, Aug./Sep. 2014, pp. 1–4.

[23] X. Z. Huang, J. Li, Q. Tan, C. M. Zhang, and L. Li, "Design principles of a phase-shift modular slotless tubular permanent magnet linear synchronous motor with three sectional primaries and analysis of its detent force," *IEEE Trans. Ind. Electron.*, vol. 65, no. 12, pp. 9346–9355, Dec. 2018.

[24] H. Zhang, B. Kou, L. Wang, Y. Jin, and H. Zhang, "A new inductance measurement method for permanent magnet synchronous linear motor," in *Proc. 17th Int. Conf. Elect. Machines Syst. (ICEMS)*, Hangzhou, China, Oct. 2014, pp. 1–4.

[25] G. Lv, D. Zeng, T. Zhou, and Z. Liu, "Investigation of forces and secondary losses in linear induction motor with the solid and laminated back iron secondary for metro," *IEEE Trans. Ind. Electron.*, vol. 64, no. 6, pp. 4382–4390, Jun. 2017.

[26] E. Severson, A. Røkke, R. Nilssen, T. Undeland, and N. Mohan, "Design and measurement of a passive thrust magnetic bearing for a bearingless motor," in *Proc. 39th Annu. Conf. IEEE Ind. Electron. Soc.*, Vienna, Austria, Nov. 2013, pp. 2720–2725.

QIANG TAN was born in Jiangsu, China, in 1991. He received the B.E. and M.E degrees in electrical engineering from the Nanjing University of Aeronautics and Astronautics, Nanjing, China, in 2014 and 2017, respectively. He is currently pursuing the Ph.D. degree with the School of Harbin Institute of Technology, Harbin, China. His current research interest is design of linear permanent magnet synchronous motors.

XUZHEN HUANG (M'14) was born in Jiangxi, China, in 1985. She received the B.E., M.E., and Ph.D. degrees from the Harbin Institute of Technology, Harbin, China, in 2006, 2008, and 2012, respectively. She is currently with the Jiangsu Key Laboratory of New Energy Generation and Power Conversion, Nanjing University of Aeronautics and Astronautics, where she is also an Associate Professor. Her current research interest includes the linear permanent magnet synchronous motors and the thermal analysis of motors.

LIYI LI was born in Heilongjiang, China, in 1969. He received the B.E., M.E., and D.E. degrees from the Harbin Institute of Technology (HIT), Harbin, China, in 1991, 1995, and 2001, respectively. He has been a Professor with the School of Electrical Engineering and Automation, HIT, since 2004. He has authored or co-authored over 110 technical papers, and holds 50 patents. His research areas are in control and drive of high-speed permanent magnet synchronous motors and linear motors.

MINGYI WANG was born in Jilin, China. He received the B.E. M.E., and D.E. degrees in electrical engineering from the Harbin Institute of Technology (HIT), Harbin, China, in 2009, 2011, and 2016, respectively. Since 2016, he has been a Lecturer with the School of Electrical Engineering and Automation, HIT. His research interests include motor drive control, power electronic applications, and magnetic levitation.